Stabilization of flat-mirror vertical-external-cavity surface-emitting lasers by spatiotemporal modulation of the pump profile

W. W. Ahmed,[1] S. Kumar,[1] R. Herrero,[1] M. Botey,[1] M. Radziunas,[2] and K. Staliunas[1,3]

[1]*Departament de Fisica i Enginyeria Nuclear, Universitat Politècnica de Catalunya (UPC), Colom 11, E-08222 Terrassa, Barcelona, Spain*

[2]*Weierstrass Institute for Applied Analysis and Stochastics, Leibniz Institute in Forschungsverbund Berlin e.V., Mohrenstrasse 39, 10117 Berlin, Germany*

[3]*Institució Catalana de Recerca i Estudis Avançats (ICREA), Passeig Lluis Companys 23, E-08010 Barcelona, Spain*

(Received 14 July 2015; published 20 October 2015)

We propose and demonstrate theoretically that vertical-external-cavity surface-emitting lasers (VECSELs) with external flat mirrors can be stabilized by applying a periodic spatiotemporal modulation of the pump current. Such pump modulation is shown to suppress the pattern-forming instabilities (modulation instabilities), which eventually results in stable beam emission. A modified Floquet linear stability analysis is used to characterize the dynamics of the modulated system and to evaluate its stabilization performance. Stability maps identify the regions in parameter space for complete and partial stabilization of VECSELs operating in different regimes depending on the external-cavity length. In particular, the stabilization method is shown to operate most efficiently in Class-A laser limit (for relatively long VECSEL resonators), while it becomes ineffective in Class-B laser limit (for relatively short resonators). The stabilization effect is further confirmed through direct integration of the dynamical equations.

DOI: 10.1103/PhysRevA.92.043829 PACS number(s): 42.65.Sf, 42.60.Lh, 05.45.−a, 42.55.Px

I. INTRODUCTION

Vertical-cavity semiconductor lasers are key sources of coherent light, especially advantageous for their compact size, high light conversion efficiency, and low lasing threshold [1]. A common classification distinguishes between few-micrometer-long vertical-cavity surface-emitting lasers (VCSELs) and vertical-external-cavity surface-emitting lasers (VECSELs), where an external cavity is used, with resonator lengths typically ranging from millimeters to centimeters [see Fig. 1(a)]. VCSELs usually suffer from dynamical spatiotemporal instabilities, which imply chaotic oscillations and result in poor spatial beam quality, even in the absence of any external perturbation. This is primarily due to the modulation instability (MI) arising from strong nonlinear effects within the cavity [2,3] and due to the absence of any intrinsic transverse mode selection mechanism. Moreover, the nonlinear destabilizing effects such as self-focusing, filamentation, and spatial hole burning are dramatically enhanced with increasing pump power [4–6]. As a result, the output power of these lasers is severely restricted, limiting their applications. Current approaches for the stabilization of the output beam's spatial structure commonly rely on external forcing techniques such as optical injection [7] and optical feedback in various configurations—spatially structured feedback [8,9], and feedback from external cavities [10,11]. All these techniques reduce the main advantage of VCSEL lasers—their compactness, and thus limit their applicability.

On the other hand, VECSELs solve the issues of transverse mode control using an output spherical mirror that ensures operation at the fundamental transverse mode [12]. However, this technique strongly limits the size of the active region, which is confined to the mode area in the center of the device, limiting the possible output power. It also introduces several disjoined elements and reduces the robustness and compactness of the device. Moreover, long external resonators and external feedback designs in these lasers lead to additional unfavorable temporal effects such as linewidth broadening, coherence collapse, and intensity noise enhancement [13,14]. The possibility to use a flat output mirror in VECSELs would allow for the realization of relatively compact and robust devices with higher output powers. However, the modulation instability problem remains to be solved in this case. Therefore, at present there is a need for finding alternative physical mechanisms to eliminate MI in VCSELs and VECSELs.

Recently, a new idea was proposed to suppress MI in a broad class of spatially extended nonlinear dynamical systems [15], relying on the introduction of a simultaneous periodic modulation in space and time. The applicability of this method, and to stabilize and improve the beam quality of light propagating in a broad area semiconductor amplifier, has already been studied in Ref. [16].

Following Ref. [15], we propose to use a periodic spatiotemporal modulation of the pump current in VECSELs to achieve a suppression of the MI of the system, leading to the stabilization of the output beam. We consider VECSELs operating in three distinct regimes: Class-A laser regime, where a centimeter-long cavity results in a photon lifetime,τ_p, longer than the nonradiative carrier recombination time,τ_N, $\tau_N \ll \tau_p$; Class-B laser regime, with micrometer-long cavities and shorter photon lifetimes,$\tau_N \gg \tau_p$; and an intermediate laser regime with $\tau_N \approx \tau_p$. The spatial field structures of all three cases can be described by the same physical model [17], due to the common nature of the active media. Relaxation oscillations do not appear for the relatively long Class-A and intermediate lasers, characterized by the values of relative carrier relaxation rate $\gamma = \tau_p/\tau_N \approx 1$–10. On the other hand, few-micrometer-long VCSELs, with τ_p and τ_N of the order of ps and ns, respectively, can be regarded as Class-B lasers [18]. As a consequence, contrary to the case of VECSELs, relaxation oscillations are inherent in VCSELs due to the small aspect ratio $\gamma \approx 0.01$. Semiconductor lasers in all the above discussed limits exhibit chaotic oscillations due to MI. Figures 1(b) and 1(c), respectively, depict the typical

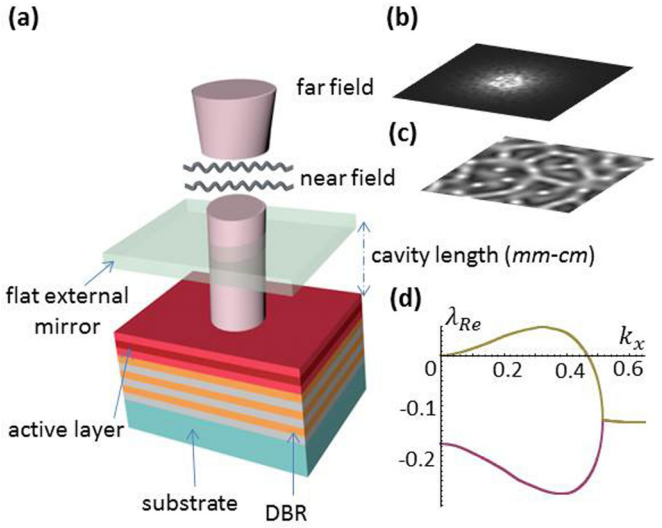

FIG. 1. (Color online) (a) Schematic diagram of a VECSEL with a flat output coupler. (b) and (c) Snapshots of the numerically calculated far and near field respectively. (d) Linear stability analysis of the steady state. The curves indicate the main Lyapunov exponents of the linearized system in dependence on the lateral perturbation wave number for $\alpha = 1.5$, $\theta = -1.5$, $C = 0.6$, $I_0 = 1.9$, $d = 0.052$, and $\gamma = 1$.

simulated far- and near-field output intensity distributions, showing chaotic optical patterns arising in dynamics.

The article is structured as follows. Section II introduces the mathematical model used to describe VECSELs, i.e., the coupled field equations for the optical field and carrier dynamics. Section III describes the modified Floquet linear stability analysis used in the study. In Sec. IV, we present a detailed analysis of VECSELs in intermediate regime ($\gamma \approx 1$) with a spatiotemporally modulated pump current. The results of the stability analysis are presented along with the results of the full numerical integration of the model equations. We explore the parameter space and identify the regions of different types of modulation instability. Sections V and VI, present the analysis for Class-A and Class-B VECSELs, respectively. Section VII explores the stability of the states according to the two-dimensional spatial model, by direct numerical integration of the model equations. Finally, Sec. VIII summarizes our findings with concluding remarks on the stabilization of considered three regimes of VECSELs.

II. MATHEMATICAL MODEL

For the description of both VECSELs and VCSELs, we consider the well-established model proposed in Ref. [17]. The mean-field dynamics of the complex field amplitude, E, and the carrier density, N, in the active region are determined by the system of coupled paraxial equations:

$$\partial_t E = -[1 + i\theta + 2C(i\alpha - 1)(N - 1)]E + i\nabla_\perp^2 E, \quad \text{(1a)}$$

$$\partial_t N = -\gamma[N - I_p + |E|^2(N - 1)] + \gamma d\nabla_\perp^2 N, \quad \text{(1b)}$$

where θ is the cavity detuning parameter, α is the linewidth enhancement factor of the semiconductor, and $\gamma = \tau_p/\tau_N$ is the carrier decay rate, normalized to the photon relaxation rate. The time, t, is normalized to the photon lifetime, $\tau_p = 2L_c/vT_c$, which depends on the transmissivity factor, T_c, velocity of light, v, and cavity length, L_c. The transverse spatial coordinates (x, y) are normalized to $\sqrt{\lambda_0 L_c/2\pi T_c}$, where λ_0 is the central wavelength of the emission. The parameter C represents the interaction between carriers and field, and depends on the laser differential gain and the photon relaxation rate. The transverse Laplacian operator, $\nabla_\perp^2$, describes the paraxial diffraction and carrier diffusion in the transverse direction. The pump current, I_p, generates the carriers within the active region, which diffuse in the transverse direction according to the diffusion factor d. The interaction between carriers and the electromagnetic field corresponds to either absorption or stimulated emission depending on the sign of the $(N - 1)$ term in Eqs. (1a) and (1b). The linewidth enhancement factor is a crucial parameter for semiconductor lasers. Note that for usual semiconductors in amplifying regimes $(N - 1) > 0$, the factor $\alpha > 0$, which leads to self-focusing effects.

III. MODIFIED FLOQUET STABILITY ANALYSIS

In order to explore the instability for the usual unmodulated VECSELs, we perform a standard linear stability analysis. For simplicity, we assume here that the model equations (1) are in one-dimensional (1D) space. We first calculate the space-homogeneous stationary solution (E_0, N_0) of the system: $N_0 = 1 + 1/2C$ and $E_0 = [(I_p - N_0)/(N_0 - 1)]^{1/2}$. Note that the field generally contains the frequency and phase factors $e^{i\omega t}$ and $e^{i\varphi}$, which can be eliminated by a suitable choice of the reference frequency or detuning, $\theta = -\alpha$, and an additional phase shift of all optical field perturbations considered below. Next, we add a small perturbation to the stationary state, $E(x,t) = E_0 + e(t)\cos(k_x x)$ and $N(x,t) = N_0 + n(t)\cos(k_x x)$, where $|e/E_0|, |n/N_0| \ll 1$, substitute these expressions into Eqs. (1), omit the higher order terms with respect to e and n, and calculate the eigenvalues of the resulting evolution equations. These eigenvalues depend on the system parameters $\theta, C, \alpha, \gamma, I_p, d$ and on the transverse wave vector, k_x. The dimension of the evolution matrix is (3×3), and expressions for the eigenvalues are explored numerically. The Lyapunov exponents which are the real parts of the eigenvalue spectrum, λ_{Re}, are plotted in Fig. 1(d). Such a spectrum is typical for a system showing unstable chaotic behavior due to the growth of modulation modes for the range of transverse wave numbers with $\lambda_{\mathrm{Re}} > 0$. The bandwidth of unstable growing modes ranges from zero to the critical wave number: $k_c = \sqrt{2\alpha(\mu - 1)/\mu}$, where $\mu = 2C(I_p - 1)$ is the scaled pump parameter such that it turns to 1 at the laser threshold [19]. For the parameters in Fig. 1, k_c is 0.47, which perfectly matches the calculated unstable region of eigenvalue curves in Fig. 1(d). It is important to note that the instability spectrum is essentially related to the dispersion of the system [15], and the region of the unstable transverse wave numbers determines the type of instability.

A periodic spatiotemporal modulation of the system can be imposed in several ways. Here, we assume a modulation of the pump current in the form

$$I_p = I_0 + 4m\cos(q_x x)\cos(\Omega t), \quad (2)$$

where m, q_x, and Ω are the amplitude and the spatial and temporal frequencies of the modulation, respectively. The

modulations are on small space and fast time scales, satisfying the conditions: $|q_x| \gg |k_x|$ and $|\Omega| \gg |\lambda|$, with k_x and λ being the typical transversal wave number and complex frequency of the growing instabilities. The modulation amplitude, m, is restricted to $4m < I_0$, in order to keep I_p positive at every instant of time, t, and at each spatial position, x. This restriction, however, can be in principle overcome by considering special and unusual configurations of VECSELs, e.g., containing an additional absorbing (unpumped) semiconductor layer, a reverse biased p-n structure, or transversally structured designs.

The $2\pi/\Omega$ time- and $2\pi/q_x$ space-periodic solution of Eqs. (1) and (2) for pump-modulated VECSELs can be expressed in terms of the spatiotemporal harmonics of the modulation with the constant amplitudes—the so-called spatiotemporal Bloch modes. For convenience, we regard such a temporally and spatially periodic state as the stationary Bloch mode solution. The resonance between the fundamental mode and the harmonics of the modulation of the pump influences the dispersion profile of the system. This resonance effect may suppress or enhance particular lateral wave numbers resulting in more or less stable perturbation modes of the system. The resonance phenomenon is most pronounced when the ratio between the temporal and square of the spatial modulation, $Q = \Omega/q_x^2$, equals, or is close to, 1; so we define Q as the resonance parameter. A detailed analysis is provided in Refs. [15,20].

Next, we numerically investigate the stability of the stationary Bloch mode solution of the 1D model with the modulated pump, using a modified Floquet method, [15]. A set of perturbations are introduced to the considered stationary Bloch mode solution, and the model equations (1) and (2) are integrated numerically over one temporal period, $T = 2\pi/\Omega$. This procedure allows us to construct the linear evolution matrix of perturbations. The eigenvalues of the resulting evolution matrix are the characteristic multipliers μ_k related to the Floquet exponents λ_k by $\mu_k = \exp(\lambda_k T)$, and to the Lyapunov exponents $\lambda_{k,\mathrm{Re}}$ which are the real parts of λ_k. The sign of the Lyapunov exponents determines the stability of the state, i.e., the exponential growth or decay of the perturbation, for positive and negative values, respectively. The state is modulationally stable only if all Lyapunov exponents are nonpositive. In the following sections, we perform this modified Floquet stability analysis for VECSELs in three characteristic regimes.

IV. INTERMEDIATE VECSELs REGIME

In the case of millimeter-long optical cavities, the normalized carrier decay rate is $\gamma \approx 1$ and VECSELs operate in a relaxation free laser regime. In the following analysis, we show that in this regime, a periodic spatiotemporal modulation of the pump current can completely stabilize the VECSELs, for appropriate modulation amplitudes and resonance parameters. We find that different sets of parameters may lead to enhancement, partial suppression, or complete suppression of the MI. The most representative cases showing the complete suppression as well as different kinds of partial suppression of instabilities are shown in Fig. 2. The red dashed

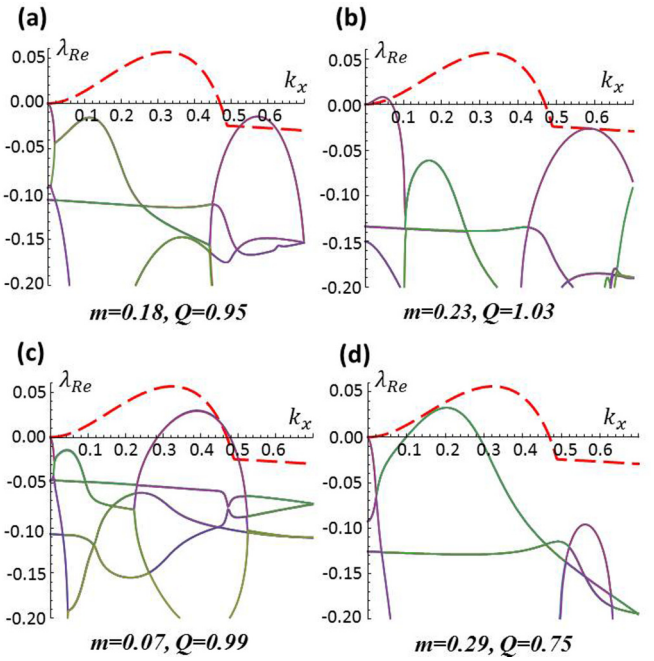

FIG. 2. (Color online) Spectra of the Lyapunov exponents for 1D modulated VECSELs in the intermediate regime as calculated numerically using the modified Floquet procedure. The parameters used are as in Fig. 1(d) with $q_x = 1.4$. Solid lines display the different branches of the Lyapunov exponents for a given parameter set (Q,m), while the dashed line represents the largest Lyapunov exponent of the nonmodulated case for comparison. Complete stabilization (a), partial stabilization with remaining weak LW (b), and SW [(c),(d)] instabilities.

curve in the figures represents the largest Lyapunov exponent of the nonmodulated (unstabilized) case for comparison. The case of complete stabilization is shown in Fig. 2(a), where all Lyapunov exponents are nonpositive. In the case of partial stabilization, the largest Lyapunov exponent for k_x from a limited interval is still positive, and weak MI is still present. The spatial instabilities are generally classified [21] as long-wavelength (LW) and short-wavelength (SW) modulation instabilities depending on whether unstable patterns arise at small k_x wave numbers [see Fig. 2(b)] or at large wave numbers [Figs. 2(c) and 2(d)].

In order to identify the regions of complete and partial stabilization, we build a stability map in the parameter space (Q,m) by color encoding the maximal Lyapunov exponent of the linear evolution matrix, $\lambda_{\mathrm{Re,\,max}} = \max_{k_x} \lambda_{\mathrm{Re}}(k_x)$, as shown in Fig. 3(a). In fact, we identify two islands of stabilization in (Q,m) space. One is located close to resonance $Q \approx 1$, and within the realistic limit of the modulation depth, $4m < I_0$ (see white area in the middle of Fig. 3). The other island is far from resonance, i.e., at $Q \approx 0.3$, and for $4m > I_0$. The white areas represent the regions of complete stabilization where all the Lyapunov exponents are nonpositive, $\lambda_{\mathrm{Re}}(k_x) \leqslant 0$. The light blue areas in the same stability map represent regions of partial stabilization, where weak LW and SW instabilities remain. The parameter sets for complete and partial stabilization discussed in Fig. 2 are indicated in the map by solid dots (a)–(d). The yellow areas in the map represent regions where we were not

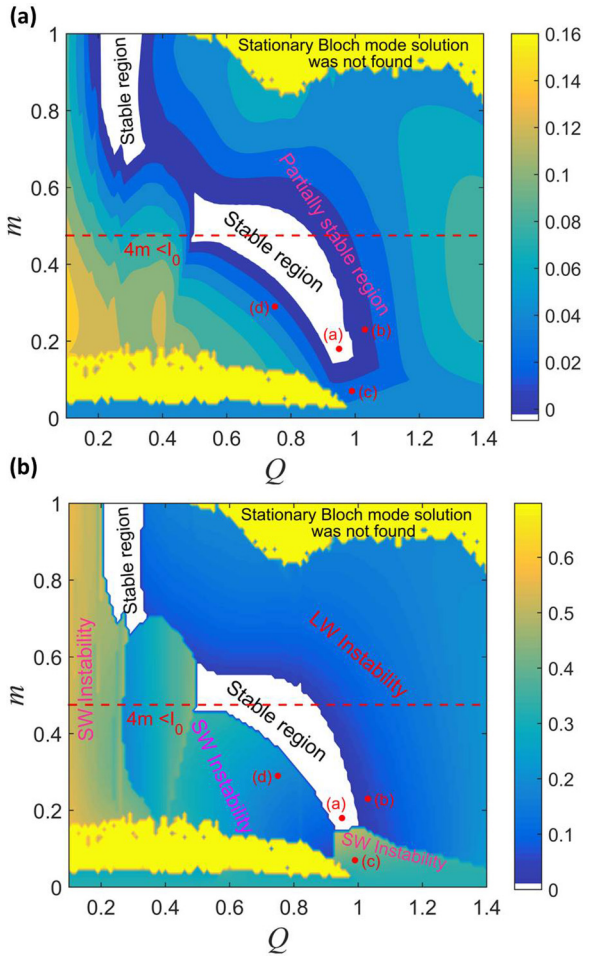

FIG. 3. (Color online) (a) Stability map for the largest Lyapunov exponent $\lambda_{\mathrm{Re,\,max}}$ in the parameter space (Q,m). (b) Map of corresponding dominant wave numbers $k_{\mathrm{Re,\,max}}$. The parameters used are as in Fig. 1(d) with $q_x = 1.4$. The limit for the modulation amplitude of common VECSEL configurations (i.e., $4m < I_0$) is represented by a horizontal red dashed line.

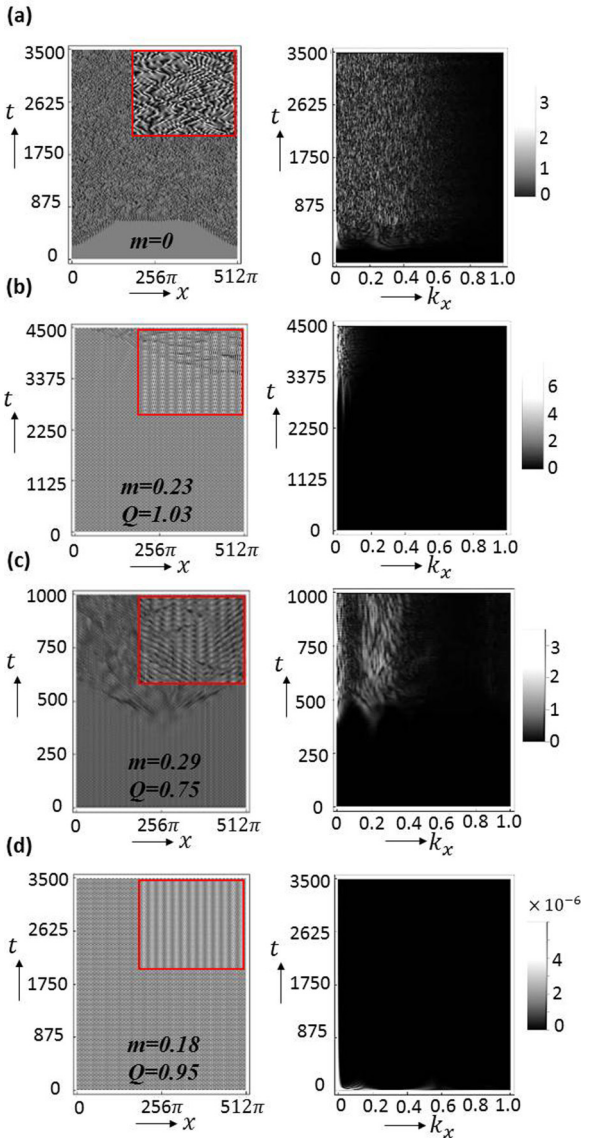

FIG. 4. (Color online) Calculated dynamics of spatiotemporally modulated VECSELs in intermediate regime according to the 1D model (1) and (2). Temporal evolution of the field intensity (left) and spatial spectrum (right). The parameters used are as in Fig. 1(d) with $q_x = 1.4$. The plots are for unmodulated (a) and modulated [(b)–(d)] cases. Full stabilization is realized in (d). The small scale modulations are filtered out for clearer representation. The insets in the left column display zoomed-in views of the field intensity.

able to locate stationary Bloch mode solution. This region is obviously excluded from the stability analysis.

In order to classify the bifurcations by crossing the boundaries of the stability balloon we explored the remaining weak instabilities: we built another map in the parameter space (Q,m), for the dominant wave number $k_{x,\,\mathrm{max}}$, defined by the relation $\lambda_{\mathrm{Re,\,max}} = \lambda_{\mathrm{Re}}(k_{x,\,\mathrm{max}})$ [see Fig. 3(b)]. The stable region is thus surrounded by the areas of partial stability with remaining LW and SW instabilities.

For the verification of the predictions of the modified Floquet linear stability analysis, we explored the spatiotemporal dynamics of the model by direct numerical integration of the 1D dynamical equations (1) and (2). The results are presented in Fig. 4.

For the unmodulated case, a typical chaotic spatiotemporal behavior is observed, as shown in Fig. 4(a). Note that the range of unstable wave numbers on the spatial spectrum [right column of Fig. 4(a)] approximately matches the region of growing perturbations in the spectra of the Lyapunov exponents from the stability analysis (red dashed curve in Fig. 2). On the other hand, we observe that for appropriate pump modulation parameters, the chaotic dynamics is reduced or eliminated, resulting in partial or complete stabilization as shown in Figs. 4(b)–4(d). As expected, no modulation modes appear in the spatial spectrum at complete stabilization [see Fig. 4(d)]. Partial stabilization is shown in Figs. 4(b) and 4(c), where the instabilities are only partially suppressed, resulting in a narrower spatial spectrum upon propagation. The remaining weak SW and LW instabilities eventually render the dynamics chaotic after a long transient time, depending on the magnitude and spectral width of the remaining instabilities. For a clearer visualization of the spatiotemporal patterns,

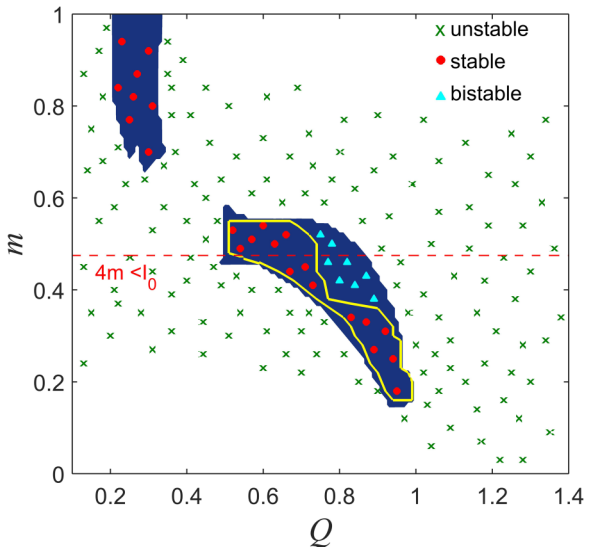

FIG. 5. (Color online) Stability map of modulated VECSELs in intermediate regime as obtained from numerical integration. The parameters used are as in Fig. 1(d) with $q_x = 1.4$. The area outside the yellow contour, but within the central blue region (indicated by triangles) represents a bistable region. Symbols: direct numerical simulations of the nonlinear system. Shaded area: stability region derived from the modified Floquet analysis.

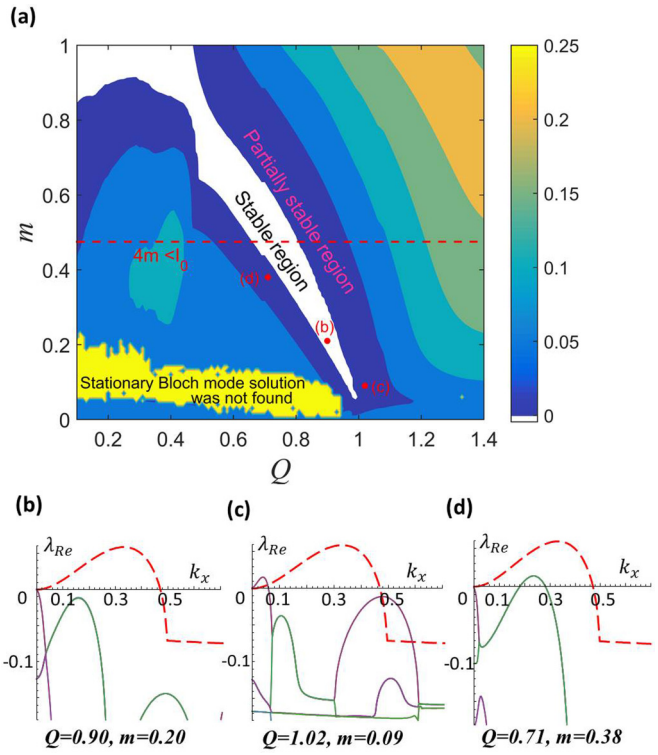

FIG. 6. (Color online) (a) Stability map for the largest Lyapunov exponent $\lambda_{\mathrm{Re,\,max}}$ in the parameter space (Q,m) for Class-A VECSELs with $\gamma = 10$ and $q_x = 1.8$. Other parameters as in Fig. 1(d). Main Lyapunov exponents (solid lines) for each particular parameter set, as compared to the largest exponent (red dashed line) of the unmodulated case. Complete and partial stabilization with remaining weak LW and SW instabilities are shown in panels (b)–(d), respectively.

a magnified view of field dynamics is provided in the insets of Fig. 4. We observe that the results obtained from direct integration of the model perfectly agree with the modified Floquet linear stability analysis.

For an extensive comparison of these results with the results of the modified Floquet stability analysis, we analyze the stability of the system at different points in the parameter space (Q,m) by direct integration. The results are summarized in Fig. 5. The system's stability is determined by observing the spatiotemporal dynamics and corresponding spatial spectrum. We consider different parameter sets (Q,m) within the specified range, following the long-time dynamics of the modulated system (typically an integration time of ~25 000 units) from the initial homogenous state, perturbed by weak random δ-correlated-in-space perturbation. The stable and unstable regimes obtained by numerical integration are indicated on the map by a solid dot (•), and a cross (×), respectively. The completely stable regions, the blue patches in Fig. 5, as obtained from the modified Floquet stability analysis, are shown in the map for comparison. Again, the stable points (•) from the numerical integration confirm the stable regime determined by stability analysis.

We have also found that within the blue shaded stabilization region in Fig. 5 at least two different regimes are possible, depending on the initial conditions: (i) the stable regime as predicted by modified Floquet analysis and (ii) turbulent regime. To identify the bistable regimes we perform simulations of Eqs. (1) and (2) for a fixed modulation amplitude m and stepwise changing (increasing and decreasing) the parameter Q. A comparison of the field dynamics for different directions of sweep of parameter Q allows us to distinguish a uniquely stable region delimited by the yellow curve and the bistable region located within the blue shaded area but outside the yellow curve. Here, depending on the initial conditions, the calculated solution was attracted either by the stable stationary Bloch mode solution, or by some chaotic attractor. Note that bistability between different spatiotemporal dynamical regimes is generally typical for an intermediate regime of VECSELs, for instance as reported in rocked VCSELs in Ref. [22].

V. CLASS-A VECSELs

Next, we investigate the stability of VECSELs in Class-A limit. In this case, the normalized carrier decay rate reaches $\gamma \approx 10$, which is only possible in centimeter-long optical cavities. This is compatible with the general conclusion that unstable spatiotemporal dynamics are more pronounced for Class-B lasers than for Class-A lasers [23]. We find that it is easier to suppress MI in this case. We perform the numerical stability analysis following the procedure as in Sec. IV and explore the parameter space (Q,m) to determine the complete and partial stabilization regions. The results are summarized in Fig. 6(a). The stability region is slightly enhanced as compared to the intermediate case of VECSELs. The spectra of the Lyapunov exponents for the most representative points (b)–(d) of the parameter space (Q,m) in Fig. 6, show either complete or partial suppression of MI.

Equations for Class-A lasers ($\gamma \approx 10$) can be simplified by adiabatically eliminating the population inversion. Particularly, for small field intensities, the model equations (1) can be reduced to a single nonlinear field equation:

$$\partial_t E = -[1 + i\theta + 2C(i\alpha - 1)(I_p - 1) \times (1 - |E|^2)]E + i\Delta_\perp^2 E, \quad (3)$$

which is known as the complex Ginzburg-Landau equation (CGLE). The complex potential of such CGLE is periodically modulated due to the modulation of the pump current. In this way, stabilization of modulated VECSELs in Class-A limit is compatible to the stabilization of the modulated CGLE [15]. Different versions of the CGLE have been derived for Class-A and Class-C laser models [24–26], in contrast to Class-B lasers where the models are not reducible to a single equation of the CGLE type [23,27].

VI. CLASS-B VECSELs

The analysis for short cavity Class-B VECSELs shows that the stabilization of VECSELs in this regime is more challenging. However, the results of the stability analysis demonstrate that full stabilization is still possible in Class-B lasers with cavity lengths down to ~100 μm. We consider a normalized carrier decay rate on the order of $\gamma \approx 0.1$, corresponding to the limiting case of a ~100-μm-long cavity. The complete suppression of MI can still be achieved for this value of γ, by an appropriate choice of the modulation parameters. In this case, higher modulation amplitudes are required as compared to Class-A and intermediate VECSELs, due to intrinsic relaxational dynamics. As shown in Fig. 7, the stabilization region in parameter space is small as compared to Class-A and intermediate VECSELs. We also note that bistability is obtained in all stabilized regimes for Class-B VECSELs (compare with Fig. 5).

VII. ANALYSIS IN 2D

Finally, we extend our analysis of VECSELs to the 2D case. Here, the modulation of the pump current in two dimensions is of the form

$$I_p = I_0 + 4[m_x \cos(q_x x) + m_y \cos(q_y y)] \cos(\Omega t), \quad (4)$$

where m_x,m_y are the modulation amplitudes along the x axis and y axis and q_x,q_y are the corresponding spatial frequencies of the modulation. Similar to the 1D case, the modulation is also considered on small space and fast time scale, hence satisfying the conditions $|q_x| \gg |k_x|$, $|q_y| \gg |k_y|$, and $|\Omega| \gg |\lambda|$ where k_x,k_y, and λ are, respectively, the typical transverse wave vectors along the x and y axis and the complex frequency of the growing instability.

For the 2D case, we limit our analysis only to the direct integration method, as the modified Floquet stability analysis entails a higher complexity in two dimensions, which is beyond the scope of this study. The typical results of numerical integration are shown in Fig. 8.

The numerically calculated patterns represent the state of the system after a long transient time ($t \sim 400$). A snapshot

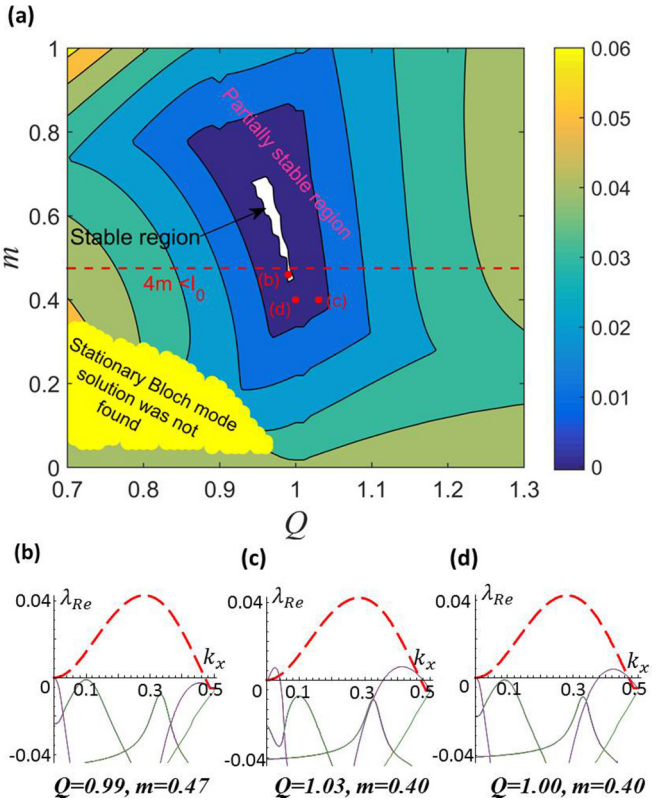

FIG. 7. (Color online) (a) Stability map for the largest Lyapunov exponent $\lambda_{\mathrm{Re,\,max}}$ in the parameter space (Q,m) for Class-B VECSELs with $\gamma = 0.1$ and $q_x = 1.0$. Other parameters as in Fig. 1(d). The other plots show the main Lyapunov exponents (solid lines) for each particular parameter set, as compared to the largest exponent (red dashed line) of the unmodulated case. Complete stabilization is obtained in (b), partial stabilization with remaining weak LW and SW instabilities in (c), and SW instability alone in (d).

of the chaotic patterns of the system for the unmodulated case is shown in Fig. 8(a). The circular disk in the corresponding spatial spectrum indicates the growth of instabilities in the system. When modulation is introduced only in one direction [see Fig. 8(b)] (i.e., $m_x \neq 0$, $m_y = 0$), we observe, as intuitively expected, the suppression of instabilities in that particular direction only [see Fig. 8(b)]. It is evident from the spatial spectrum that the circular disk is fragmented due to the suppression of instabilities along the modulated axis while the remaining instabilities along the vertical direction generate the resultant partially chaotic pattern. Next, we consider modulation with a square symmetry $m_x = m_y$ for different modulation parameters. A partial stabilization of the system is achieved for the amplitudes $m_x = m_y = 0.21$ as shown in Fig. 8(c). Here, a weak, slowly growing MI disrupts the square symmetric pattern after a long time of propagation. This weak instability is seen more clearly in the spectrum of Fig. 8(c). For the modulation amplitude, $m_x = m_y = 0.15$, we observe complete stabilization of the system, as shown in Fig. 8(d), where the square pattern remains stable even after a long transient time. The general conclusion from 2D simulations is that the stabilization studied in the 1D case works also for 2D cases. The 2D modulation offers richer possibilities

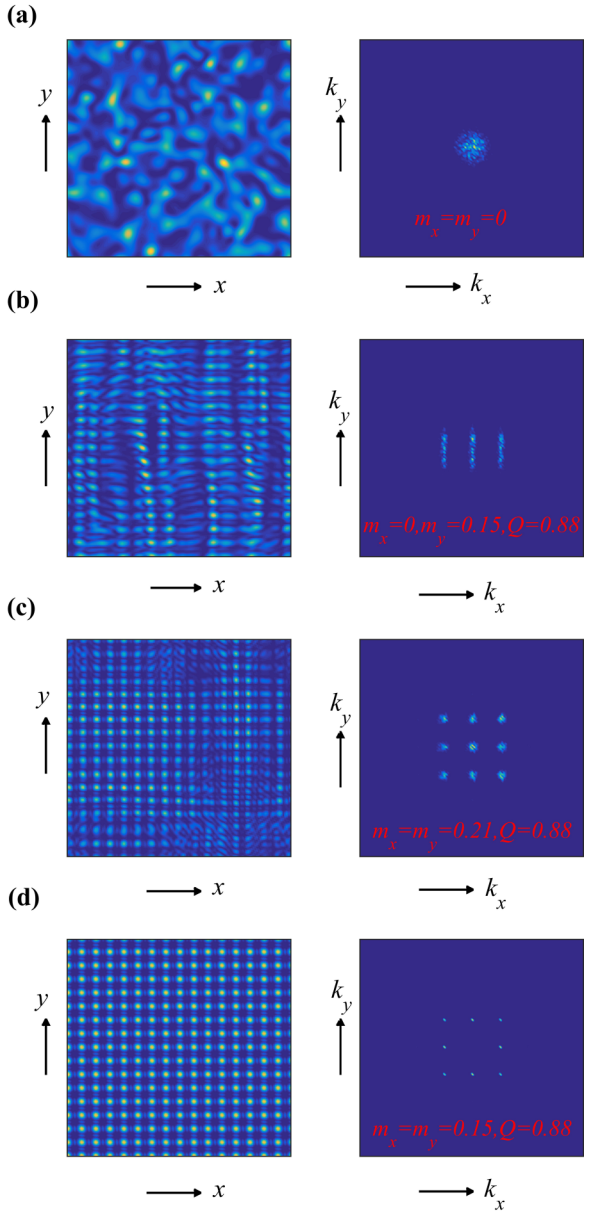

FIG. 8. (Color online) Numerically calculated snapshots of the intensity distribution patterns after a long transient time ($t \sim 400$) for the 2D model, showing field intensity (left) and spatial spectrum (right). The parameters are as in Fig. 1(d) and the size of integration window is 100×100. (a) Chaotic intensity distributions and corresponding spectra for the unmodulated system. (b) Suppression of MI only in the horizontal direction. (c) Partial stabilization in both spatial directions for a weak square symmetric modulation and (d) complete stabilization for a square symmetric modulation of appropriate amplitude.

than the 1D case: different wave numbers of q_x and q_y can be considered in the case of a rectangular modulation pattern; also different geometries of modulations (hexagonal, octagonal, etc.) can be considered. The detailed analysis of different 2D modulation specifics is out of the scope of this article and requires a separate study.

VIII. CONCLUSIONS

Summarizing, we theoretically analyze the stabilization of flat-mirror VECSELs by a spatiotemporal modulation of the pump current. Indeed, we show that the intercoupling of the spatial and temporal modes of the modulation can suppress MI in VECSELs. This effect can contribute to enhance the stability of such lasers at higher powers and improve the spatial quality of the output beam. By using a modified Floquet analysis and direct integration methods, we calculate the MI free operating regions, in parameter space, for VECSELs operating in different regimes. We pay special attention to the case of intermediate VECSELs, as the stabilization in this regime is expected to have an important technological impact. We show that Class-A VECSELs can also be efficiently stabilized, thus making the proposed stabilization technique well suitable for quantum dot VECSELs (which are characterized by significantly large values of the carrier decay rate [28]). Short cavity, Class-B laser VECSELs (and VCSELs) limit the stabilization, since only lasers with length cavities down to around 100 μm can be completely stabilized by the proposed method.

Long cavity VECSELs are not compact light sources and can therefore be stabilized by other means, such as by using curved mirrors, as discussed in the Introduction. On the contrary, we show that VECSELs of $\sim$1 mm cavity length, referred to as the intermediate case throughout the article, can be efficiently stabilized by the proposed method. Note that, in this last case, no other regularization mechanisms (e.g., curved mirrors) are applicable. The estimated frequency and period of the modulation required for the stabilization of VECSELs in such intermediate regimes are experimentally still achievable, being on the order of 10 GHz and 100 μm, respectively.

ACKNOWLEDGMENTS

We acknowledge financial support by Spanish Ministerio de Educación y Ciencia and European FEDER (project FIS2011-29734-C02-01). The work of M.R. was supported by the Einstein Center for Mathematics Berlin under project D-OT2. W.W.A. was supported by the Erasmus Mundus Doctorate Program Europhotonics (Grant No. 159224-1-2009-1-FR-ERA MUNDUS-EMJD).

[1] K. Iga, F. Koyama, and S. Kinoshita, IEEE J. Quantum Electron. **24**, 1845 (1988).
[2] J. Ohtsubo, *Semiconductor Lasers: Stability, Instability and Chaos*, 3rd ed. (Springer, Berlin, 2013).
[3] G. H. M. Van Tartwijk and G. P. Agrawal, Prog. Quantum Electron. **22**, 43 (1998).
[4] J. R. Marciante and G. P. Agrawal, IEEE J. Quantum Electron. **32**, 590 (1996).
[5] H. Adachihara, P. Ru, J. V. Moloney, O. Hess, and E. Abraham, J. Opt. Soc. Am. B **10**, 658 (1993).
[6] A. Valle, J. Sarma, and K. A. Shore, IEEE J. Quantum Electron. **31**, 1423 (1995).

[7] S. Takimoto, T. Tachikawa, R. Shogenji, and J. Ohtsubo, IEEE Photon. Technol. Lett. **21**, 1051 (2009).
[8] S. K. Mandre, I. Fischer, and W. Elsäßer, Opt. Lett. **28**, 1135 (2003).
[9] C. Simmendinger, D. Preisser, and O. Hess, Opt. Express **5**, 48 (1999).
[10] J. Martin-Regalado, G. H. M. van Tartwijk, S. Balle, and M. San Miguel, Phys. Rev. A **54**, 5386 (1996).
[11] M. Munkel, F. Kaiser, and O. Hess, Phys. Rev. E **56**, 3868 (1997).
[12] A. C. Tropper and S. Hoogland, Prog. Quantum Electron. **30**, 1 (2006).
[13] J. Y. Law and G. P. Agrawal, J. Opt. Soc. Am. B **15**, 562 (1998).
[14] K. P. Ho, J. D. Walker, and J. M. Kahn, IEEE Photon. Technol. Lett. **5**, 892 (1993).
[15] S. Kumar, R. Herrero, M. Botey, and K. Staliunas, Sci. Rep. **5**, 13268 (2015).
[16] S. Kumar, R. Herrero, M. Botey, and K. Staliunas, Opt. Lett. **39**, 5598 (2014).
[17] L. Spinelli, G. Tissoni, M. Brambilla, F. Prati, and L. A. Lugiato, Phys. Rev. A **58**, 2542 (1998).
[18] A. Uchida, *Optical Communication with Chaotic Oscillations: Application of Non-Linear Dynamics and Synchronization* (Wiley, Weinheim, 2012).
[19] F. Prati and L. Columbo, Phys. Rev. A **75**, 053811 (2007).
[20] M. Radziunas, M. Botey, R. Herrero, and K. Staliunas, Appl. Phys. Lett. **103**, 132101 (2013).
[21] M. C. Cross and P. C. Hohenberg, Rev. Mod. Phys. **65**, 851 (1993).
[22] C. Fernandez-Oto, G. J. de Valcarcel, M. Tlidi, K. Panajotov, and K. Staliunas, Phys. Rev. A **89**, 055802 (2014).
[23] K. Staliunas and V. J. Sánchez-Morcillo, *Transverse Patterns in Nonlinear Optical Resonators* (Springer, Berlin, 2003).
[24] P. Coullet, L. Gil, and F. Rocca, Opt. Commun. **73**, 403 (1989).
[25] G.-L. Oppo, G. D'Alessandro, and W. J. Firth, Phys. Rev. A **44**, 4712 (1991).
[26] K. Staliunas, Phys. Rev. A **48**, 1573 (1993).
[27] G.-L. Oppo, A. M. Yao, F. Prati, and G. J. de Valcárcel, Phys. Rev. A **79**, 033824 (2009).
[28] C. Shan, X. Zhao, M. Hu, C.-H. Shek, and W. Huang, Front. Optoelectron. **5**, 157 (2012).